



JOURNAL OF
APPLIED
CRYSTALLOGRAPHY

Volume 53 (2020)

Supporting information for article:

A thermal gradient approach to variable temperature measurements resolved in space

Daniel O'Nolan, Guanglong Huang, Gabrielle E. Kamm, Antonin Grenier, Chia-Hao Liu, Paul Todd, Allison Wustrow, Gia Thinh Tran, David Montiel, James R Neilson, Simon J. L. Billinge, Peter J. Chupas, Katsuyo S. Thornton and Karena W. Chapman

A thermal gradient approach to variable temperature measurements resolved in space

Daniel O'Nolan^a, Guanglong Huang^b, Gabrielle E. Kamm^a, Antonin Grenier^a, Chia-Hao Liu^c, Paul Todd^d, Allison Wustrow^d, Gia Thinh Tran^d, David Montiel^b, James R Neilson^d, Simon J. L. Billinge^c, Peter J. Chupas^a, Katsuyo S. Thornton^b and Karena W. Chapman^{a*}

^aDepartment of Chemistry, Stony Brook University, 100 Nicolls Rd, Stony Brook, New York, 11794, USA

^bDepartment of Mechanical Engineering, University of Michigan, Ann Arbor, Michigan, 48109, USA

^cDepartment of Materials Science & Engineering, Columbia University, New York, New York, 10027, USA

^dDepartment of Chemistry, Colorado State University, Fort Collins, Colorado, 80523, USA

Correspondence email: karena.chapman@stonybrook.edu

S1. Thermal Modelling

S1.1. Thermal Model

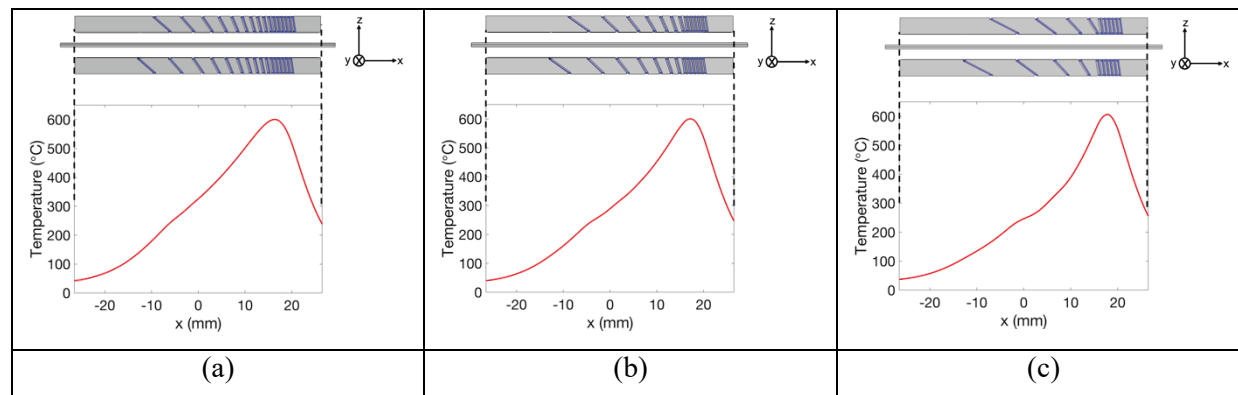


Figure S1 The predicted temperature profile for the sample when wires are coiled around the heating element in three different manners. The grooves that face the sample are along the *y*-direction (into the figure).

The thermal conduction between the surfaces of wires and heating elements that are in direct contact, as well as within the bulk of each object, is described by

$$\rho C_p \frac{\partial T}{\partial t} - k \nabla^2 T = Q, \quad (1)$$

where ρ is the density, C_p is the heat capacity, T is the temperature, t is time, k is the thermal conductivity and Q is the power density from a source within the bulk. For the heating elements and the sample, $Q = 0$. For the wires, Q is the power density from Joule heating, as described by

$$Q = \mathbf{i} \cdot \mathbf{E} = \kappa |\nabla \phi|^2, \quad (2)$$

where \mathbf{i} is the current density, \mathbf{E} is the electric field, κ is the electrical conductivity, and ϕ is the electric potential.

Surface-to-surface thermal radiation (Evans *et al.*, 1997, Modest, 2013) is considered between each pair of surfaces facing each other but not in direct contact. We consider a point, P , on one of these surfaces, which we denote as the surface of interest, S . The net outgoing radiative heat flux, J , at this point is given by

$$J(\mathbf{r}_P) = (1 - \alpha)G(\mathbf{r}_P) + \epsilon e_b(T(\mathbf{r}_P)), \quad (3)$$

where \mathbf{r}_P indicates the position of point P , α is the absorptivity (assumed to be equal to emissivity, ϵ , in this model) of surface S , and G is the incident radiative flux onto the surface at point P . The first term in Eq. (3) accounts for reflection at point P on S . The second term accounts for emission, where $e_b(T)$ is the radiant emittance, given by the Stefan–Boltzmann law:

$$e_b(T) = \sigma T^4, \quad (4)$$

where σ is the Stefan–Boltzmann constant. The spatial dependence of variables indicated in Eq (3) is omitted below for simplicity. The flux, G , at point P on S is given by

$$G = \int_{S'} \frac{(-\mathbf{n}' \cdot \mathbf{r})(\mathbf{n} \cdot \mathbf{r})}{\pi |\mathbf{r}|^4} J' dS' + \left(1 - \int_{S'} \frac{(-\mathbf{n}' \cdot \mathbf{r})(\mathbf{n} \cdot \mathbf{r})}{\pi |\mathbf{r}|^4} dS'\right) e_b(T_{amb}). \quad (5)$$

The first term in Eq. (5) accounts for radiation from all unobstructed surrounding surfaces, S' , that are facing the surface of interest, S . The second term accounts for incident ambient radiation. The vector, \mathbf{r} , points from point P on S to a point P' on S' , \mathbf{n} and \mathbf{n}' are the outward normal vectors at P and P' , respectively, T_{amb} is the ambient temperature far from the apparatus (assumed to be 20 °C), and J' is the net outgoing heat flux from P' on S' . The ambient view factor, $1 - \int_{S'} \frac{(-\mathbf{n}' \cdot \mathbf{r})(\mathbf{n} \cdot \mathbf{r})}{\pi |\mathbf{r}|^4} ds'$, accounts for the fraction of ambient radiation on P that is not blocked by S' .

The boundary conditions on the surface of each object are obtained via the sum of contributions from each of the heat transfer mechanisms involved. For the surfaces that face each other from the heating elements, the wires, and the sample, the heat flux onto the surface S due to surface-to-surface thermal radiation, $-\mathbf{n} \cdot \mathbf{q}_{ss}$, is given by

$$-\mathbf{n} \cdot \mathbf{q}_{ss} = G - J = \epsilon(G - e_b(T)). \quad (6)$$

The surfaces of the heating elements and wires that are not facing each other or facing the sample radiate energy to the surrounding environment. Therefore, surface-to-ambient thermal radiation is considered for those surfaces:

$$-\mathbf{n} \cdot \mathbf{q}_{sa} = \epsilon\sigma(T_{amb}^4 - T^4). \quad (7)$$

For all the surfaces of the heating elements that are in contact with the air, Newton's law of cooling with constant heat transfer coefficient is applied in addition to the thermal radiation:

$$-\mathbf{n} \cdot \mathbf{q}_{air} = h(T_{amb} - T), \quad (8)$$

where h is the heat transfer coefficient between an object's surface and air, which is a fitting parameter.

The heat transfer mechanisms considered in the model are surface-to-surface radiation, conduction, and Newton's law of cooling. For the simplicity in building the geometry, the wire is approximated as a square rod, rather than a cylinder. We assume that two sides of the wire are in perfect contact with the grooves and, thus heat conduction is applied for these boundaries. The remaining two sides of the wire that are not in contact with the grooves radiate heat to the heating elements and the sample. We assume that the quartz capillary is transparent to radiation and that heat conduction between the sample and the quartz capillary is poor; therefore, the capillary is omitted in the model. We also omit the sample holder from the simulation geometry because it is not in direct contact with the sample but rather it is separated from the sample by the capillary.

Table S1 The parameters employed in the simulation, as well as their literature values and sources where available, are presented. The temperatures associated with the literature values ranged from 20°C to 1000°C, which are provided along with parameter values.

Parameters	Value employed in the model	Units	Source	Range of values in literature
Ceramic bars				
Heat capacity	7.75×10^2	J/kgK	Literature ¹	7.75×10^2 (@ 25 °C, Al ₂ O ₃) – 1.27×10^3 (@ 976.85 °C, Al ₂ O ₃) (Ditmars et al., 1982)

¹ The lower bound from the literature is selected.

Thermal conductivity	0.55	W/mK	Fitting	0.1 (@ 298.15 °C, Al ₂ O ₃) (Shimizu et al., 2013) – 2.0 (@ 726.85 °C, silica) (Jund & Jullien, 1999)
Density	1.2×10^3	kg/m ³	Experiment	1.2×10^3
Surface emissivity	0.3	--	Fitting	0.2 (oxidized aluminum) – 0.79 (silica) (Emissivity Coefficients Materials., 2003)
Heat transfer coefficient	33	W/m ² K	Fitting	$0.5 - 10^3$ (Janiak, 2003)
Ceramic bars (used for parameterization)				
Length	38.7	mm	Experiment	--
Width	3.6	mm	Experiment	--
Depth	8.4	mm	Experiment	--
Ceramic bars (used for Mark 2A, 2B and 2C)				
Length	53	mm	--	--
Width	3.5	mm	--	--
Depth	8.5	mm	--	--
Heating wires				
Heat capacity	4.6×10^2	J/kgK	Literature ¹	4.6×10^2 (@ 20 °C) – 7.2×10^2 (@ 1000 °C) (Kanthal® A-1 resistance heating wire and resistance wire, 2018)
Thermal conductivity	20	W/mK	Fitting	11 (@ 50 °C) – 26 (@ 1000 °C) (Kanthal® A-1 resistance heating wire and resistance wire, 2018)

Density	7.1×10^3	kg/m ³	Literature	7.1×10^3 (Kanthal® A-1 resistance heating wire and resistance wire, 2018)
Surface emissivity	0.7	--	Literature	0.7 (Kanthal® A-1 resistance heating wire and resistance wire, 2018)
Electrical conductivity	Interpolation ²	S/m	Literature	6.63×10^5 (@ 1000 °C) – 6.90×10^5 (@ 20 °C) (Kanthal® A-1 resistance heating wire and resistance wire, 2018)
Cross-sectional area	8×10^{-2}	mm ²	Literature	8×10^{-2} (Matsuda <i>et al.</i> , 2004)
Heat transfer coefficient	33	W/m ² K	Fitting	0.5 – 10 ³ (Janiak, 2003)
Applied voltage (for parameterization)	16	V	Experiment ³	16 – 19
Applied voltage (for Mark 2A)	14.95	V	--	--
Applied voltage (for Mark 2B)	13	V	--	--
Applied voltage (for Mark 2C in Figure 5 (left))	10.85	V	--	--
Applied voltage (for Mark 2C, original width in Figure 5 (middle))	16	V	--	--

2 The temperature-dependent electrical conductivity in our model is interpolated using piecewise cubic functions based on the data in the literature.

3 The lower bound from the experimental values is selected.

Applied voltage (for Mark 2C, doubled width in Figure 5 (middle))	24	V	--	--
Applied voltage (for Mark 2C, half width in Figure 5 (middle))	12.6	V	--	--
NaCl/Si mixture sample powder				
Heat capacity	8.6×10^2	J/kgK	Literature ¹	8.6×10^2 (@ 31.25 °C, NaCl) – 1.0×10^3 (@ 499.35 °C, NaCl) (Leadbetter et al., 1969)
Thermal conductivity	0.35	W/mK	Fitting	0.13 (@ 26.85 °C, NaCl) (Murashov & White, 2000) – 1.56×10^2 (@ 26.85 °C, Si) (Glassbrenner & Slack, 1964)
Density	2.17×10^3	kg/m ³	Literature ¹	2.17×10^3 (NaCl) (Haynes, 2013 - 2014) – 2.32×10^3 (Si) (Endo et al., 2003)
Surface emissivity	0.45	--	Fitting	0.1 (@ 269.85 °C, Si) – 0.7 (@ 599.85 °C, Si) (Ravindra et al., 2001, Satō, 1967)
Radius	0.45	mm	Experiment	--
Distance between surfaces of two heating elements that face each other	6.35	mm	Experiment	--
Length (for parametrization)	50	mm	Estimated ⁴	--

⁴ The length of the sample was measured in comparison with the heating elements; the length value does not influence the resulting thermal profile if it is longer than the heating elements.

Length (for Mark 2A, 2B and 2C)	60	mm	--	--
------------------------------------	----	----	----	----

S2. Non-negative Matrix Factorization

Given a dataset of m observed data, each in n dimension, the data can be regarded as a data matrix M with dimension $n \times m$. In the context of NMF, we are seeking an approximation of M , where:

$$M \approx M^e W \quad (9)$$

with a basis matrix M^e and weight matrix W . The dimensions of M and W are $n \times p$ and $p \times m$, respectively and mostly importantly $p < m$. The values for the matrices M^e and W that provide the best approximation in Eq. 9 can be solved by minimizing

$$\|M - M^e W\|_F \quad (10)$$

while keeping M^e and W non-negative and $\|\cdot\|_F$ indicates the Frobenius norm.(Lee & Seung, 2001, Wang & Zhang, 2013) The p columns of M^e form the basis of this approximation and each column of W represents the projected weight of each observed data on this basis. By constraining $p < m$, the NMF is likely to extract components that are descriptive across entire dataset.

S3. Supplementary References

COMSOL Multiphysics® v. 5.4. www.comsol.com. COMSOL AB, Stockholm, Sweden

Emissivity Coefficients Materials., (2003). https://www.engineeringtoolbox.com/emissivity-coefficients-d_447.html

Kanthal® A-1 resistance heating wire and resistance wire (2018). KANTHAL.